COMMUNICATION

Check for updates

Microfluidic synthesis of monodisperse and size-tunable CsPbBr₃ supraparticles†

Julia Nette,[a] Federico Montanarella,[bc] Chenglian Zhu,[bc] Taras V. Sekh,[bc] Simon C. Boehme, ID [bc] Maryna I. Bodnarchuk,[bc] Gabriele Rainò,[bc] Philip D. Howes, ID [d] Maksym V. Kovalenko ID [bc] and Andrew J. deMello ID *[a]

The highly controlled, microfluidic template-assisted self-assembly of CsPbBr₃ nanocrystals into spherical supraparticles is presented, achieving precise control over average supraparticle size through the variation of nanocrystal concentration and droplet size; thus facilitating the synthesis of highly monodisperse, sub-micron supraparticles (with diameters between 280 and 700 nm).

The spontaneous assembly of materials into ordered superstructures (self-assembly) has long been of interest in the scientific community, as it combines the individual properties of the building blocks with the interdependent structural properties of the formed superstructure, enabling the union of self-contained properties from different building blocks.[1] For example, semiconductor nanocrystals (NCs) can self-assemble into NC-superstructures exhibiting long-range order, with various morphologies and sizes, forming 1D, 2D or 3D superstructures.[2] Such structures can be prepared *via* evaporation or destabilization.[3–5] Whilst evaporation typically produces thin films of NC superstructures, destabilization yields superstructures in a solution phase, with the particle assembly induced by introduction of a non-solvent that changes the particle solubility in the dispersed medium.

To date, these fabrication methods have not been successful in producing monodisperse and size-controlled 3D confined superstructures or supraparticles (SPs). In addition to evaporation and destabilization, other preparation methods such as gravitational sedimentation,[6] spontaneous and template-driven self-assembly[7,8] have also been investigated. Interestingly, template-driven assembly,

where the template determines the size and morphology of the assembly, has been shown to yield greater control over the size and morphology of the formed superstructures.[9,10] The assembly of building blocks into SPs is particularly interesting since their solution stability can simplify further processing. Superstructures self-assembled from colloidal NCs have been the subject of much interest, as they combine the properties of their component building blocks with the tuneable structural properties of the higher-order structure. Indeed, semiconducting NCs exhibit remarkable optical properties, with their highly tuneable emission and near-unity photoluminescence quantum yields (PLQYs) being desirable in applications such as lighting, optoelectronics and biomedical sensing.[11,12] These optical properties can be fully used and adjusted in ordered structures, unlocking new and desirable optical properties,[6,13] such as the coupling of the individual NC emissions into a single red-shifted superfluorescence pulse.[3,4] Other properties include lasing,[14] excitonic coupling,[15] whispering gallery modes,[14,16] photonic effects,[15] and white light emission.[17]

Lead halide perovskite NCs are ideal building blocks for forming self-assembled superstructures, owing to their outstanding optical and electronic properties. Such properties include high absorption coefficients, high brightness, narrow band-edge emission and size- and composition-tuneable emission.[18,19] A number of CsPbBr₃ NC superstructures have been reported in the literature,[3,20–28] with quasi-atomic NC behaviour in the superlattice, in addition to exhibiting excitonic coupling and superfluorescence.[3,4,22] In this regard, an oil-in-oil templating approach for making CsPbBr₃ SPs has been presented by Tang and co-workers.[21] Specifically, the authors reported the fabrication of CsPbBr₃ SPs *via* an oil-in-oil emulsification approach, using a fluorinated solvent (FC-40) and fluorinated surfactants. Whilst interesting, vortex-based mixing of the two phases results in polydisperse droplet populations and thus yields polydisperse SPs. In general, the optical properties of superstructures are often determined by the quality of the assembly process, which is enabled by precise control over both particle size and superstructure morphology. Unsurprisingly, the ability to make small and monodisperse

[a] Institute of Chemical and Bioengineering, Department of Chemistry and Applied Biosciences, ETH Zurich, Zurich 8093, Switzerland.
E-mail: andrew.demello@chem.ethz.ch
[b] Institute of Inorganic Chemistry, Department of Chemistry and Applied Biosciences, ETH Zurich, Zurich 8093, Switzerland
[c] Laboratory for Thin Films and Photovoltaics, Empa – Swiss Federal Laboratories for Materials Science and Technology, Dübendorf CH-8600, Switzerland
[d] Division of Mechanical Engineering and Design, London South Bank University, 103 Borough Road, London SE1 0AA, UK
† Electronic supplementary information (ESI) available. See DOI: https://doi.org/10.1039/d3cc00093a

SPs has become an important issue, which we tackle here by leveraging droplet-based microfluidic reactors. Microfluidic technologies have been shown to be highly useful in the generation of small, monodisperse SPs. In microfluidic environments, enhanced mass- and thermal transport allow for precise control over both the reaction- and flow-conditions.[29] For example, Montanarella et al.[14] presented a droplet-based microfluidic reactor for the synthesis of monodisperse CdSe/CdS SPs between 5 and 15 μm size, with an average diameter of 10.2 ± 0.5 μm. Specifically, the authors used a templating approach, where NC building blocks were encapsulated within cyclohexane droplets using a co-flow microfluidic geometry and then delivered into a vial containing a water solution saturated with cyclohexane. Stirring of this solution at room temperature for between 6 and 18 hours yielded monodisperse SPs dispersed in water. Additionally, Marino and co-workers[30] reported the microfluidic fabrication of SPs using a "source-sink" emulsion approach, in which an emulsion containing both toluene droplets with NCs ('source') and hexadecane droplets ('sink') is formed. Here, hexadecane droplets swell with toluene, whilst toluene droplets decrease in size until solid SPs are formed. Finally, it is also noted that a templating-based microfluidic method for the fabrication of monodisperse SPs has been reported for the preparation of magnetic particles with average diameters of 25 μm.[31,32] Herein, we demonstrate the production of monodisperse $CsPbBr_3$ SPs using a droplet-based microfluidic reactor that engenders precise control over SP size (Fig. 1). $CsPbBr_3$ SPs are formed via NC self-assembly from a colloidal suspension of $CsPbBr_3$ NCs. A glass microfluidic device, integrating a 5 μm-wide flow focusing nozzle, is used to produce monodisperse droplets with diameters between 3 and 5 μm and volumes between 8 and 37 fL (Table S1 and Fig. S4, ESI†), comprising a colloidal suspension of $CsPbBr_3$ NCs with didodecyldimethylammonium (DDAB) ligands in toluene (see ESI† for details), stabilized and encapsulated within a surfactant-loaded (5 w%) fluorinated oil (FC-40). This assembly method is inspired by the flask-based oil-in-oil templating approach reported by Tang and co-workers,[21] with particles being formed via spherical confinement induced by

solvent evaporation over a 48-hour period. Importantly, the microfluidic device maintained stable flow conditions over extended periods of time, and enabled direct control over both droplet size and droplet-size distributions (Table S1 and Fig. S4, ESI†).

SP populations formed in this manner exhibit low polydispersity, with a size distribution below 14% (Table S1, ESI†). This can largely be attributed to the stability of the droplet generation process, with microfluidically-produced droplets showing minimal variations in diameter over a 12-hour period; for example, droplets produced with an initial diameter of 3.78 μm $\pm$ 0.39 μm, exhibited an average diameter of 3.50 μm $\pm$ 0.33 μm after 12 hours of continuous operation (Fig. S1, ESI†). Control of the SP size was achieved by varying the droplet size and the concentration of NCs in toluene (Fig. 2). Droplet diameters could be tuned from 3.1 μm $\pm$ 0.31 μm to 4.78 μm $\pm$ 0.38 μm by changing either the total volumetric flowrate or the volumetric flowrate ratio between the carrier fluid and the NCs in toluene. The accessible range of droplet diameters is primarily defined by the dimensions of the flow focusing nozzle, and thus larger or smaller droplets could be formed using alternate chip geometries. NC concentrations were varied between 2.15 mg mL^{-1} and 7.3 mg mL^{-1} (Fig. S3, ESI†). At concentrations above 7.3 mg mL^{-1}, the droplets were unstable. At concentrations below 2.15 mg mL^{-1}, SPs did not form perfectly resulting in hollow SPs (Fig. S2, ESI†). This combination of accessible droplet sizes and NC concentrations allowed SP volumes to be tuned between ca. 0.02 and 0.2 μm^3 (diameters between ca. 280 and 700 nm). Accordingly, SPs can be tailored to interact with specific parts of the visible range.

The produced SPs exhibit low polydispersity and are spherical in shape, with an exemplary circularity of 0.356 and a roundness of 0.978 (Fig. S7, ESI†), and a size distribution that was retained from the microfluidic droplets (Table S1 and Fig. S4, ESI†). In this template-driven approach, the SP shape is guided by droplet shape (spherical), through the self-assembly of cubic NCs (Fig. S5, ESI†). SEM images (Fig. 3a and b) confirm that SPs are spherical and highly ordered. NCs assemble in a simple cubic pattern with distortions that can be ascribed to spherical confinement.
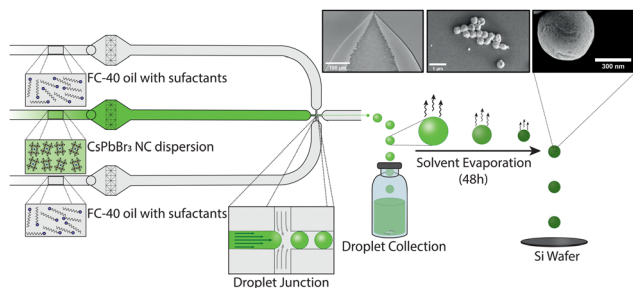

Fig. 1 Schematic of the microfluidic workflow used to synthesize $CsPbBr_3$ SPs, with inset images displaying a high-speed camera image of droplet formation, an SEM image of multiple solid SPs and a single solid SP. Droplet generation occurs at a 5 μm-wide flow focusing nozzle producing. Droplets are monodisperse, with diameters between 3 and 5 μm, and contain a dispersion of $CsPbBr_3$ NCs in toluene encapsulated by a surfactant-laden FC-40 oil continuous phase.
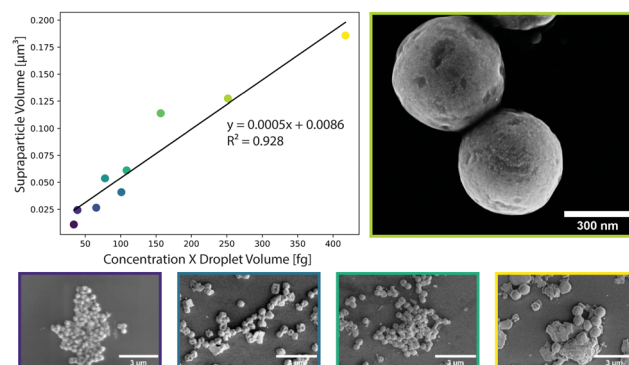

Fig. 2 Control of average SP size (volume) through variation of NC concentration and droplet volume. Linear dependency between SP volume and NC concentration multiplied by droplet volume and SEM images of SPs at selected positions colour-coded.
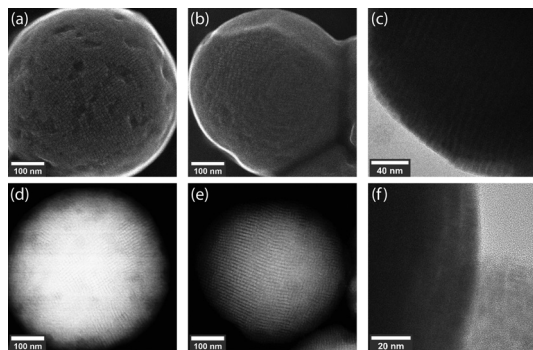
Fig. 3 Structural characterization of two SPs *via* SEM imaging (a and b), Secondary Electron (SE) STEM imaging (d and e) and high-resolution Transmission Electron Microscopy (HRTEM) imaging (c and f). In SEM/SE STEM images, the disordered simple cubic arrangement of the NCs in the SPs can be seen.
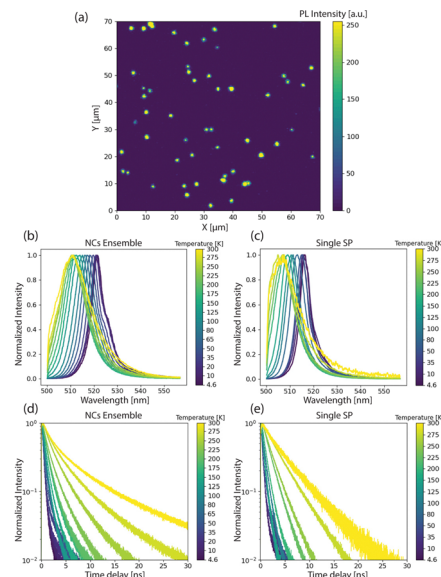

Fig. 4 Optical characterization of SPs and disordered NC ensembles *via* time-integrated and time-resolved PL. (a) PL intensity image of several single CsPbBr$_3$ SPs on a silicon substrate at 300 K (b) PL spectra of a disordered NC ensemble (*i.e.* dropcasted thin film) at temperatures between 4.6 K and 300 K (c) PL spectra of a single SP between 4.6 K and 300 K (d) PL decay profiles of a disordered NC ensemble between 4.6 K and 300 K, (e) PL decay profiles of a single SP between 4.6 and 300 K.

Secondary-electron scanning transmission electron microscopy (SE STEM) images presented in Fig. 3d and e show well-ordered NC superlattices, with the NCs assuming a distorted simple cubic lattice. The size and shape of the cubic NCs is unchanged after self-assembly (Fig. 3c, f and Fig. S5, ESI†); the representative particles shown in Fig. 3 have an average diameter of 624 nm $\pm$ 56 nm. The SP shape is always spherical, reproducible across various NC and SP samples and independent of the SP. This is in contrast to prior observations by Tang and co-workers.[21] In this regard, it is likely that the high interfacial tension associated with toluene droplets and the 5% surfactant oil solution induces strain on the NCs, and thus distortion during self-assembly. The formation of spherical SPs guided by droplet shape may appear counterintuitive when using cubic nanocrystals as building blocks. However, a similar phenomenon has been reported by Wang and co-workers when synthesizing spherical SPs from Fe$_x$O/CoFe$_3$O$_4$ nanocubes.[33] Furthermore, cubic SPs or 2D superlattices have been reported when CsPbBr$_3$ nanocubes form SPs through self-assembly *via* evaporation.[3,20]

Next, to probe the fundamental optical properties of the microfluidically-generated SPs, we investigated the time-integrated and time-resolved photoluminescence (PL) of single SPs and the component NCs at temperatures between 4.6 K and 300 K. As shown in Fig. 4a, confocal PL imaging (λ_{ex} = 405 nm) reveals that SPs are suitably distributed for single-SP measurements, with SP-to-SP distances exceeding 2 µm for the vast majority of collected SPs. At 4.6 K, the disordered NC ensemble, obtained *via* drop-casting as a thin film, emits at 522 nm, with single SPs showing a slightly blue-shifted emission at 517 nm (Fig. 4b and c blue lines). This variation in peak emission could be attributed to (i) more pronounced reabsorption, (ii) a larger size distribution of the NCs, and/or (iii) a different dielectric environment within the disordered film. Fig. 4d and e present temperature-dependent time-resolved PL decay profiles for both disordered NCs ensembles and single SPs. At 4.6 K, fits of the decays associated with both species feature a common short lifetime component of approximately 400 ps, similar to the decay time of single NCs of comparable size.[34] Upon heating, single SPs exhibit qualitatively similar temperature-dependent behaviour as the disordered NC ensemble. First, as

shown in Fig. 4b and c, in both samples the PL emission peak continuously shifts to higher energy and, the PL linewidth increases, as a result of lattice expansion and thermal broadening, respectively. Second, as shown in Fig. 4d lifetimes reach 2–4 ns at 300 K. This observation is consistent with Diroll *et al.*,[35] who reported an increase in the average PL lifetime in CsPbBr$_3$ NCs upon increasing the temperature from 2.7 K to 300 K. At 300 K, however, a markedly different behaviour emerges between both samples. Fig. 4d highlights significant deviations from single-exponential decay kinetics for the disordered NC ensemble, suggesting distinct lifetime components that originate from differently sized NCs within the population, and with larger NCs possessing longer lifetimes at 300 K.[36] In contrast, the PL decay associated with single SPs at 300 K is mono-exponential in nature (red line in Fig. 4e), which likely indicates a much narrower size distribution within the SP population. Overall, SPs share the common properties of CsPbBr$_3$ NC building blocks, such as bright and fast emission, and narrow bandwidth PL. Enabled by our control over SP size and polydispersity, the already mentioned large range of optoelectronic applications can be further expanded and developed, for example by utilizing the combination of superior optical properties of the individual NCs and the collective behaviour achieved *via* suitable structural and photonic engineering *via* superstructures.[15]

To conclude, we have presented the first synthesis of sub-micron, highly monodisperse, spherical SPs from CsPbBr$_3$ NCs *via* a microfluidic oil-in-oil templating approach. The microfluidic templating method allows for precise control over the size of the formed supraparticles, through variations in both droplet size and the concentration of building blocks within

each droplet. This provides for size tuneability across the range of the whole visible spectrum. Additionally, adoption of a microfluidic workflow ensures low polydispersity (below 14%) in droplet size, which directly translates into SPs with a small SP size distribution, and direct control over SP size. The obtained consist of unscathed NCs (with retained optical properties) that assemble into a distorted simple cubic lattice. Using our microfluidic self-assembly method, the size and shape of SPs can be directly controlled by the droplet template. We expect that use of this technique will facilitate the study of superfluorescence in small structures, and help to explore the limits of this elusive phenomenon.

Conflicts of interest

There are no conflicts to declare.

Notes and references

1 O. Chen, L. Riedemann, F. Etoc, H. Herrmann, M. Coppey, M. Barch, C. T. Farrar, J. Zhao, O. T. Bruns, H. Wei, P. Guo, J. Cui, R. Jensen, Y. Chen, D. K. Harris, J. M. Cordero, Z. Wang, A. Jasanoff, D. Fukumura, R. Reimer, M. Dahan, R. K. Jain and M. G. Bawendi, *Nat. Commun.*, 2014, **5**, 5093.

2 E. Penzo, A. Loiudice, E. S. Barnard, N. J. Borys, M. J. Jurow, M. Lorenzon, I. Rajzbaum, E. K. Wong, Y. Liu, A. M. Schwartzberg, S. Cabrini, S. Whitelam, R. Buonsanti and A. Weber-Bargioni, *ACS Nano*, 2020, **14**, 6999–7007.

3 G. Rainò, M. A. Becker, M. I. Bodnarchuk, R. F. Mahrt, M. V. Kovalenko and T. Stöferle, *Nature*, 2018, **563**, 671–675.

4 G. Rainò, H. Utzat, M. G. Bawendi and M. V. Kovalenko, *MRS Bull.*, 2020, **45**, 841–848.

5 F. Montanarella, J. J. Geuchies, T. Dasgupta, P. T. Prins, C. Van Overbeek, R. Dattani, P. Baesjou, M. Dijkstra, A. V. Petukhov, A. Van Blaaderen and D. Vanmaekelbergh, *Nano Lett.*, 2018, **18**, 3675–3681.

6 M. A. Boles, M. Engel and D. V. Talapin, *Chem. Rev.*, 2016, **116**, 11220–11289.

7 D. García-Lojo, S. Núñez-Sánchez, S. Gómez-Graña, M. Grzelczak, I. Pastoriza-Santos, J. Pérez-Juste and L. M. Liz-Marzán, *Acc. Chem. Res.*, 2019, **52**, 1855–1864.

8 E. Marino, E. Marino, A. W. Keller, D. An, S. Van Dongen, S. Van Dongen, T. E. Kodger, K. E. MacArthur, M. Heggen, C. R. Kagan, C. R. Kagan, C. R. Kagan, C. B. Murray, C. B. Murray and P. Schall, *J. Phys. Chem. C*, 2020, **124**, 11256–11264.

9 S. Wintzheimer, T. Granath, M. Oppmann, T. Kister, T. Thai, T. Kraus, N. Vogel and K. Mandel, *ACS Nano*, 2018, **12**, 5093–5120.

10 F. Bertolotti, A. Vivani, F. Ferri, P. Anzini, A. Cervellino, M. I. Bodnarchuk, G. Nedelcu, C. Bernasconi, M. V. Kovalenko, N. Masciocchi and A. Guagliardi, *Chem. Mater.*, 2022, **34**, 594–608.

11 M. V. Kovalenko, L. Manna, A. Cabot, Z. Hens, D. V. Talapin, C. R. Kagan, V. I. Klimov, A. L. Rogach, P. Reiss, D. J. Milliron, P. Guyot-Sionnnest, G. Konstantatos, W. J. Parak, T. Hyeon, B. A. Korgel, C. B. Murray and W. Heiss, *ACS Nano*, 2015, **9**, 1012–1057.

12 F. Montanarella and M. V. Kovalenko, *ACS Nano*, 2022, **16**, 5085–5102.

13 B. De Nijs, S. Dussi, F. Smallenburg, J. D. Meeldijk, D. J. Groenendijk, L. Filion, A. Imhof, A. Van Blaaderen and M. Dijkstra, *Nat. Mater.*, 2015, **14**, 56–60.

14 F. Montanarella, D. Urbonas, L. Chadwick, P. G. Moerman, P. J. Baesjou, R. F. Mahrt, A. Van Blaaderen, T. Stöferle and D. Vanmaekelbergh, *ACS Nano*, 2018, **12**, 12788–12794.

15 E. Marino, A. Sciortino, A. Berkhout, K. E. MacArthur, M. Heggen, T. Gregorkiewicz, T. E. Kodger, A. Capretti, C. B. Murray, A. Femius Koenderink, F. Messina and P. Schall, *ACS Nano*, 2020, **14**, 13806–13815.

16 D. Vanmaekelbergh, L. K. Van Vugt, H. E. Bakker, F. T. Rabouw, B. De Nijs, R. J. A. Van Dijk-Moes, M. A. Van Huis, P. J. Baesjou and A. Van Blaaderen, *ACS Nano*, 2015, **9**, 3942–3950.

17 F. Montanarella, T. Altantzis, D. Zanaga, F. T. Rabouw, S. Bals, P. Baesjou, D. Vanmaekelbergh and A. Van Blaaderen, *ACS Nano*, 2017, **11**, 9136–9142.

18 G. Rainò, N. Yazdani, S. C. Boehme, M. Kober-Czerny, C. Zhu, F. Krieg, M. D. Rossell, R. Erni, V. Wood, I. Infante and M. V. Kovalenko, *Nat. Commun.*, 2022, **13**, 2587.

19 L. Protesescu, S. Yakunin, M. I. Bodnarchuk, F. Krieg, R. Caputo, C. H. Hendon, R. X. Yang, A. Walsh and M. V. Kovalenko, *Nano Lett.*, 2015, **15**, 3692–3696.

20 J. S. Van Der Burgt, J. J. Geuchies, B. Van Der Meer, H. Vanrompay, D. Zanaga, Y. Zhang, W. Albrecht, A. V. Petukhov, L. Filion, S. Bals, I. Swart and D. Vanmaekelbergh, *J. Phys. Chem. C*, 2018, **122**, 15706–15712.

21 Y. Tang, L. Gomez, A. Lesage, E. Marino, T. E. Kodger, J. M. Meijer, P. Kolpakov, J. Meng, K. Zheng, T. Gregorkiewicz and P. Schall, *Nano Lett.*, 2020, **20**, 5997–6004.

22 I. Cherniukh, G. Rainò, T. Stöferle, M. Burian, A. Travesset, D. Naumenko, H. Amenitsch, R. Erni, R. F. Mahrt, M. I. Bodnarchuk and M. V. Kovalenko, *Nature*, 2021, **593**, 535–542.

23 A. Pan, M. J. Jurow, F. Qiu, J. Yang, B. Ren, J. J. Urban, L. He and Y. Liu, *Nano Lett.*, 2017, **17**, 6759–6765.

24 M. V. Kovalenko and M. I. Bodnarchuk, *Chimia*, 2017, **71**, 461–470.

25 Z. Zhang, B. Wang, H. B. Zhao, J. F. Liao, Z. C. Zhou, T. Liu, B. He, Q. Wei, S. Chen, H. Y. Chen, D. Bin Kuang, Y. Li and G. Xing, *Appl. Catal. B Environ.*, 2022, **312**, 121358.

26 Y. X. Feng, G. X. Dong, K. Su, Z. L. Liu, W. Zhang, M. Zhang and T. B. Lu, *J. Energy Chem.*, 2022, **69**, 348–355.

27 C. Zhou, Y. Zhong, H. Dong, W. Zheng, J. Tan, Q. Jie, A. Pan, L. Zhang and W. Xie, *Nat. Commun.*, 2020, **11**, 329.

28 D. Vila-Liarte, M. W. Feil, A. Manzi, J. L. Garcia-Pomar, H. Huang, M. Döblinger, L. M. Liz-Marzán, J. Feldmann, L. Polavarapu and A. Mihi, *Angew. Chem., Int. Ed.*, 2020, **59**, 17750–17756.

29 H. Q. Chen, X. Y. Wang, H. K. Bisoyi, L. J. Chen and Q. Li, *Langmuir*, 2021, **37**, 3789–3807.

30 E. Marino, S. W. Van Dongen, S. J. Neuhaus, W. Li, A. W. Keller, C. R. Kagan, T. E. Kodger and C. B. Murray, *Chem. Mater.*, 2022, **34**, 2779–2789.

31 J. R. Morillas, E. Carreón-González and J. de Vicente, *Soft Matter*, 2021, **17**, 3733–3744.

32 Q. Fu, Y. Sheng, H. Tang, Z. Zhu, M. Ruan, W. Xu, Y. Zhu and Z. Tang, *ACS Nano*, 2015, **9**, 172–179.

33 D. Wang, M. Hermes, R. Kotni, Y. Wu, N. Tasios, Y. Liu, B. De Nijs, E. B. Van Der Wee, C. B. Murray, M. Dijkstra and A. Van Blaaderen, *Nat. Commun.*, 2018, **9**, 2228.

34 M. A. Becker, R. Vaxenburg, G. Nedelcu, P. C. Sercel, A. Shabaev, M. J. Mehl, J. G. Michopoulos, S. G. Lambrakos, N. Bernstein, J. L. Lyons, T. Stöferle, R. F. Mahrt, M. V. Kovalenko, D. J. Norris, G. Rainò and A. L. Efros, *Nature*, 2018, **553**, 189–193.

35 B. T. Diroll, H. Zhou and R. D. Schaller, *Adv. Funct. Mater.*, 2018, **28**, 1800945.

36 F. Krieg, P. C. Sercel, M. Burian, H. Andrusiv, M. I. Bodnarchuk, T. Stöferle, R. F. Mahrt, D. Naumenko, H. Amenitsch, G. Rainò and M. V. Kovalenko, *ACS Cent. Sci.*, 2021, **7**, 135–144.